J Seismol
https://doi.org/10.1007/s10950-024-10233-4

RESEARCH

Unraveling the unusual 22 November 2020 earthquake (Mw 3.5) in the Nile Delta Hinge Zone: Origin and tectonic implications

I.F Abu El Nader · Hany M. Hassan · Hazem Badreldin · Adel S. Othman · Ashraf Adly

Received: 4 January 2024 / Accepted: 17 July 2024

Abstract On November 22, 2020, a moment magnitude of Mw 3.5 earthquake struck the highly populated Nile Delta. This event marked the first recorded earthquake in this area. We employed the polarity of P and S wave first motions, as well as SH and SV amplitudes and their respective ratios (SH/P and SV/SH), to constrain the focal mechanism solution. Furthermore, considering Brune's circular source model, kinematic source parameters were estimated through spectral analysis of available and reliable seismic data. The obtained solution reveals an oblique-slip fault mechanism, characterized by strike, dip, and rake angles of 341º, 69º, and -47º, respectively. Additionally, the two fault planes exhibit trends aligned with the E-W and NNW directions. This normal fault mechanism with a strike component aligns with previously identified events in various active areas of Egypt, indicating a dominant extensional stress regime. The trend/plunge of the P and T axes are determined to be 299º/46º and 42º/13º, respectively. Moreover, the NE trending of the T axis agrees well with the current extension stress field prevalent along the eastern border of Egypt. The average seismic moment and moment magnitude values for P and SH waves are estimated to be 1.86×10^{14} Nm, and 3.5, respectively. Furthermore, the average source values of radius and stress drop are calculated to be 304 m, and 29 bar, respectively. Through a comparative and comprehensive analysis of fault mechanism solutions in the Nile Delta region and its surroundings, we have concluded that the fault structures in the Hinge Zone and Cairo-Suez Shear Zone exhibit similarities. This finding provides evidence that the geodynamic processes and fault style are identical. In conclusion, the provided information contributes to our understanding of the seismotectonic characteristics and earthquake hazard in the epicentral region. Moreover, this study serves as a motivation for future site response and seismic hazard analyses based on a scenario-based approach.

Keywords The Nile Delta earthquake · Source mechanism · Seismic moment · Seismotectonics · Hinge Zone

I. Abu El Nader · H. M. Hassan (✉) · H. Badreldin · A. S. Othman · A. Adly
National Research Institute of Astronomy and Geophysics (NRIAG), Helwan 11421, Egypt
e-mail: helsayed@ogs.it; hany_hassan@nriag.sci.eg

I. Abu El Nader
e-mail: iman.abuelnadr@nriag.sci.eg

H. Badreldin
e-mail: hbadreldin@ogs.it

A. S. Othman
e-mail: adelsami@nriag.sci.eg

H. M. Hassan · H. Badreldin
National Institute of Oceanography and Applied Geophysics (OGS), Trieste, Italy
e-mail: hbadreldin@ogs.it

A. S. Othman
Alma Mater Studiorum - University of Bologna, Department of Physics and Astronomy "Augusto Righi" (DIFA), Bologna, Italy

Published online: 06 August 2024

1 Introduction

The Nile Delta earthquake on 22 November 2020 (at 11:52:11 UTC) is considered the first instrumentally recorded event in the central part of the Nile Delta. This earthquake was well-recorded by the Egyptian National Seismic Network (ENSN) and Egyptian Strong Motion Network (ESMN) operated by the National Research Institute of Astronomy and Geophysics (NRIAG). In this work, we present a detailed analysis of this earthquake.

Its epicenter is located about 16km southeast of Mansoura city (Table 1 and Fig. 1) within the Nile Delta seismic sub-network. The earthquake was widely felt in almost most of the Nile Delta cities of the Nile Delta without any reported casualties or damage, but it caused significant concern about its implications. No historical earthquakes have been reported in close proximity to the location of this recent event.

The epicentral area, with an estimated population of more than 500 k within a 25 km radius according to the latest 2022 (CAPMAS 2022) census (Central Agency for Public Mobilization and Statistics), is characterized by high population exposure, building vulnerability, and high socio-economic importance. Moreover, subsurface of the Nile Valley and Delta are made of soft thick sediment which can severely increase the ground motion amplitude and duration and produce undesirable amplification (e.g. El-Sayed et al. 2001; El-Sayed et al. 2004). However, proactive preparedness and mitigation efforts based on adequately understanding the region's seismotectonic setting and seismic hazards can help dense cities, e.g., Mansoura, reduce future earthquake losses.

The 22 November 2020 earthquake was located within an area tectonically known as the Nile Delta's Hinge zone (Fig. 1). Recent studies on crustal deformation in Egypt have provided insights into the contemporary deformation occurring in the Nile Delta (e.g. Saleh and Becker 2015; Rashwan et al. 2021). These studies have indicated a complex pattern of subsidence in both the horizontal and vertical components of the delta. The subsidence in the area is influenced by various factors, including anthropic, stratigraphic, and tectonic factors, as highlighted by Stanley (1988). Notably, the northeastern part of the Nile Delta exhibits higher subsidence rates compared to the northwestern part, as previously observed by Saleh and Becker (2019). Rashwan et al. (2021) further supported these findings by reporting a significant mean subsidence rate of approximately 11 mm/year at the GPS station in Mansoura.

Geological studies have revealed the presence of multiple fault systems within the Hinge Zone, including both extensional and strike-slip faults (Fig. 1). However, the verification of these findings through earthquake analysis has been limited, as significant seismic activity had not been observed until the occurrence of the earthquake on November 22, 2020. Consequently, this study relies on analyzing a single earthquake, highlighting the need for a detailed investigation of source characterization to enhance our understanding of seismotectonics and conduct seismic hazard analysis in anticipation of more significant earthquakes. The seismotectonic implications of the Nile Delta Hinge Zone are of great concern due to its proximity to densely populated areas. The presence of active faults within the hinge zone signifies the potential for seismic hazards and the occurrence of earthquakes.

However, this earthquake is considered a small-size earthquake, investigating its source characteristics and seismotectonic is crucial for understanding hazard and risk mitigation for a couple of purposes as it occurred along the Hinge Zone of the Nile Delta. First, the epicentral location of the earthquake occurred in a densely populated area. The second reason is our need to better understand its source characteristics in light of the seismotectonic of the Hinge Zone, which is usually considered as relatively tectonically stable area (no seismogenic source was

Table 1 Earthquake Parameters of the Nile Delta Hinge Zone Earthquake. (ERH = error in horizontal component; ERZ = error in vertical component)

Date DD/MM/YYYY	O.T HH:MM: SS	LAT N°	LONG E°	Depth km	RMS	ERH km	ERZ km	Magnitude (ML)
22/11/2020	09:52:10.87	30.909	31.25	18	0.22	0.85	1.62	3.3

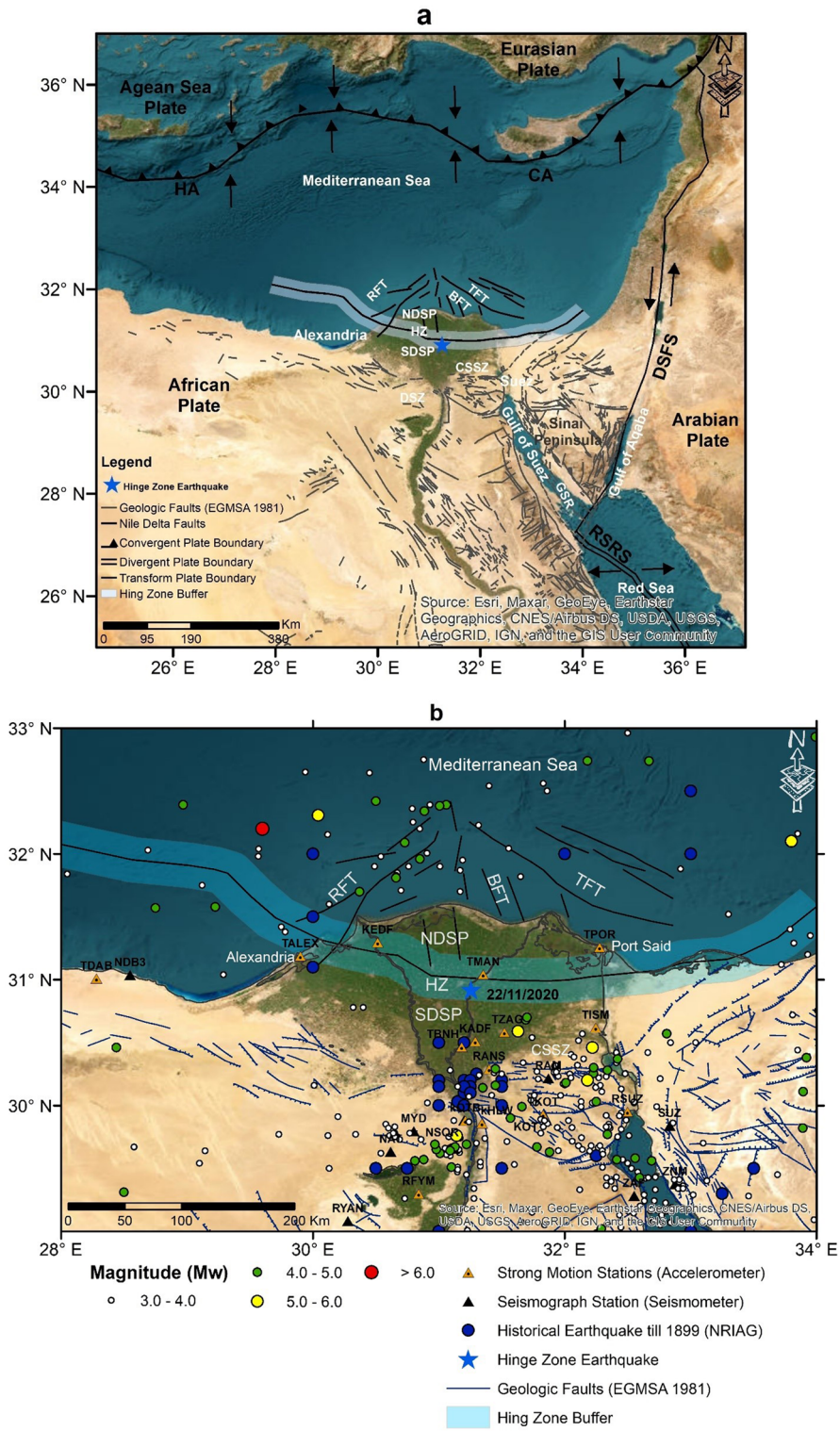

Fig. 1 **a** depicts the general regional tectonic map highlighting the major active plate boundaries, while Figure (**b**) shows the distribution of historical earthquakes and regional instrumental seismicity from 1900 to 2020 around the Nile Delta region (updated historical earthquake catalog compiled by NRIAG in 2010). The Blue star marks the epicenter of the 22nd November 2020 earthquake. HA and CA represent the Hellenic Arc and Cyprian Arc, respectively. The geological and tectonic characteristics are derived from the Egyptian Geological Survey and Mining Authority (EGSMA 1981), along with studies by Hussein and Abd-Allah (2001) and Hassan et al. (2021), which are properly referenced therein. The abbreviations are as follows: RSRS—Red Sea Rift System, DSFS—Dead Sea Fault System, GSR—Gulf of Suez Rift, CSSZ—Cairo-Suez Shear Zone, DSZ—Dahshour Source Zone, NDSP—North Delta Structural Province, SDSP—Southern Delta Structural Province, HZ—Nile Delta's Hinge Zone, RFT—Rosetta Fault Trend, TFT—Temsah Fault Trend, and BFT—Bardawil Fault Trend

delineated for this part) and considered as seismically silent during the past decades that subjected to instrumental monitoring. Therefore, the main aim of this work is to investigate the nature of this first instrumentally recorded event. The focal mechanism solution and source parameters of this unusual source are estimated by analyzing the waveform data of the strong and weak motion networks operated by NRIAG. Thus, the comprehensive and comparative analysis of this recent event could assist in understanding the seismotectonic setting of the region with the final aim of properly estimating seismic hazards and minimizing earthquake impacts.

2 Geological, structural and tectonic characteristics of the Nile *Delta*: A regional and local perspective

The Nile Delta region is located in the northeastern part of the African continent and surrounded by three main tectonic elements (Fig. 1a): the African-Eurasian plate margin, the Red Sea and Gulf of Suez rift system and the Gulf of Aqaba-Dead Sea fault system. The present-day tectonic deformation and seismicity within the region is considered as a manifestation for the interaction and the relative motion along these boundaries and their distant effects, through stresses transmitted across the plates to weak zones in the lithosphere.

The Red Sea rift system is an ongoing continental rift and active sea-floor spreading and it has been formed due to the relative movements between African and Arabian plates. The rift system was formed by early anticlockwise rotation of the Arabian plate from the African plate. It divides at the northern end into two parts: Gulf of Suez rift and the Gulf of Aqaba (sinistral shear). Two types of faults are found in the recently active Gulf of Aqaba: strike-slip and dip-slip normal faults trending towards N-S and NNE-SSW. These trends are correlated to the cracks system of different orientations found in the rocks on both flanks and as well as within the Gulf, as reported by many authors (e.g. Klinger et al. 1999).

The Gulf of Suez represents the northern extension of the Red Sea rifting. Both stratigraphic and structural studies show that the Red Sea and the Gulf of Suez rifting began in Oligocene time and developed in the Miocene (Said 1990). It represents the northwestern branch of the Sinai triple junction together with the Gulf of Aqaba and the Red Sea. Two major sets of fault patterns have clearly influenced the rifting processes, i.e. the main NW Clysmic and the transfer trends.

Moustafa and Abd-Allah (1992) attributed the northern termination of the Suez rift to the northwestward as a transfer of throw from the northern part of the rift into the Cairo-Suez Shear Zone (CSSZ) via east–west oriented pre-rift faults. They also indicated an ending of the NNW-SSE faults along western Sinai against the east–west Themed fault. The CSSZ is geographically extends over the northern part of Eastern Desert of Egypt and covers the area that extends from the northern end of the Suez rift to the Nile valley. This zone is affected by the late Oligocene-early Miocene deformation related to the opening of the Gulf of Suez in response to ENE-WSW oriented extension. Meanwhile, it is probable that a part of this deformation is transferred to the land and led to the rejuvenation of the deep-seated preexisting E-W oriented faults by dextral transition (oblique-slip movement) in addition to NW–SE striking faults (Moustafa and Abd-Allah 1992). This produced E-W elongated belts of left stepped en-echelon normal faults of about 20km width, overlie preexisting deep-seated faults of right lateral strike slip movement (e.g. Khalil and McClay 2002; Abd-Allah et al. 2012). The CSSZ on this basis is characterized by several E-W elongated belts of E-W to WNW normal faults having left stepped arrangement.

The Dahshour seismic source (DSS) is located in the northern part of the Western Desert, which generally forms an unstable shelf (Said 1990), further to the west of the CSSZ. The predominant structural features in this zone are faults. Abou Elenean et al. (2010) indicated that this area is seismically active, as evidenced by the occurrence of small to moderate earthquakes. Notably, the strongest instrumentally recorded earthquake in this zone occurred in October 12, 1992, with observed magnitudes of approximately mb5.8. The spatial distribution of earthquakes reveals that their epicenters align along a north–south direction. Abu El Nader (2010) studied the focal mechanism solutions for several earthquakes in this zone and concluded that the solutions vary from pure dip-slip to pure strike-slip.

The major morphostructural domains in the southeastern Mediterranean Sea are the Mediterranean Ridge and the Nile Deep Sea Fan. The Nile Deep Sea

Fan is bounded by the Dead Sea shear zone to the east, the Cyprus convergent zone, and the Mediterranean Ridge to the north. The Egyptian continental margin is situated south of the folded arc forming the Mediterranean Ridge, encompassing features such as the Nile Deep Sea Fan, Eratosthenes Seamount, and Herodotus Basin. This margin varies significantly in width from east to west (Korrat et al. 2005). The continental margin, a zone of weakness, experienced crustal thinning during the Triassic period. This transitional zone, between the faulted continental crusts, is oriented N110–120E and may be prone to reactivation with dextral strike-slip and reverse fault components (Korrat et al. 2005; Abu El Nader et al. 2013).

The Nile Delta basin is well defined by its highly complicated structural framework due to its location along the northeast African plate and the southeast of the Mediterranean region. Consequently, it is mainly affected by the structural setting and tectonic regime of the two regions. It is also situated along the continental margin basin, which was developed due to the separation of the Afro-Arabian plate from the Eurasian plate in the Early Cretaceous time (Stanley 1988). The geology and tectonic history of the Nile Delta region have been the subject of considerable investigations (e.g. Ross and Uchupi 1977:1985; Said 2012; Shalaby and Sarhan 2023). The main structural trends of the Nile Delta have been recognized by Sestini (1989) and Zaghloul et al. (2001). Among these trends are: 1) **East–West or Tethyan Trend**: This trend likely relates to the original continental margin rifting in the south-eastern Mediterranean during the early Mesozoic. Notable examples include the Oligo-Miocene Hinge Zone, Mit Ghamr Fault, and the northern and southern flexures of the onshore Nile Delta; 2) **Northeast-Southwest or Rosetta Fault Trend (RFT)**: Originating in the Late Cretaceous, this trend is comprises the Pelusium, Qattara-Eratosthenes, and Gamasa fault lines. These faults likely originated from a single point in the northeast corner of the Mediterranean Sea near Alexandria. Additionally, they exhibit sinistral strike-slip displacement; 3) **Northwest-Southeast Trend**: Active during the Miocene, this trend is best represented by the Temsah or Bardawil trends in the eastern offshore Nile Delta. Most faults within this trend northward at approximately 45°W, although some follow the Clysmic trend of the Gulf of Suez and the Red Sea, trending about north 30°W.

Through thorough surface and subsurface geological and structural mapping, researchers have classified the Nile Delta region into three distinct structural-sedimentary provinces (Sestini 1989; Hussein and Abd-Allah 2001). These provinces, i.e., southern Nile Delta and northern Nile Delta and faults trending east–west separate these provinces, forming the Hinge Zone (see Fig. 1a) (e.g. Hussein and Abd-Allah 2001; Harms and Wray 1990). Recent geophysical, geologic, and structural investigations (e.g. Barakat 2010; Hassan et al. 2021) indicated that the width of this Hinge Zone is estimated to be 30-40 km wide (Fig. 1a). Also, it represents an east-to-west continuation of the Levant hinge line across the North Delta Block.

Investigations on seismic and borehole data along the Hinge Zone revealed a complex system of faults, including normal listric, slumping, and growth faults (Sestini 1989; Harms & Wray 1990; Barakat 2010). These faults exhibit considerable displacements (Sestini 1989) and contribute to the gradual thickening of sediments along the coastal sections of the Nile Delta and its fan. According to Hassan et al. (2021), the Southern Delta structural province is characterized by a sedimentary section approximately 1–1.5 km thick composed of post-Eocene clastics, and the Northern Delta structural province, which consists of Neogene sediments in a section ranging from 4 to 6 km thick. Also, one of the important findings is that the Hinge Zone is characterized by extensional tectonics.

2.1 Southern Nile *Delta* structural province

The Southern Nile Delta province (SDSP) (south Delta block in Said 2012) extends northward from the east–west trending faults bounding the northern part of the Cairo-Suez Province to the Nile Delta's Hinge Zone (Fig. 1a). This province is entirely covered by Pliocene–Quaternary sediments. Structurally, several east–west orientated faults divide the province from south to north into the Bitter Lake graben and Ismailia horst. The southern Delta structural province is characterized by the imprint of the late Cretaceous Syrian arc folding, considered its main tectonic feature. Three main fault lines are intersecting this province i.e., the Pelusium shear, the Gulf of Suez-Cairo-Alexandria, and the Sebennetic faults. These faults converge at a triaxial junction near Cairo.

2.2 Northern Nile *Delta* structural province

The northern Nile Delta structural province (NDSP) lies north of the Hinge Zone and extends beyond the northern boundary of the study area (Fig. 1a). The Northern Delta province, a Levant basin subunit, is considered the most active tectonic province of the Nile Delta. The NDSP is dissected by several east–west-trending listric normal faults that bound southward tilted fault blocks of half-grabens. Oligocene and Miocene rocks filled the low areas between rotated blocks, creating several east–west elongated wedge-shaped basins (Fig. 1a). In the northernmost part of the study area, the Oligocene and Miocene rocks are affected by north–south to north-northwest, northwest, and northeast to north-northeast-orientated faults. These faults, designated as BFT, TFT, and RFT, respectively, are illustrated in Fig. 1a. This province's structural style and deformation closely resemble those in the following.

2.3 Nile *Delta* Hinge's Zone

The Nile Delta's Hinge Zone (HZ) plays a critical role in the tectonic evolution of the delta and significantly influences the overall facies variations of the African continental margin within the study area. This zone is characterized by a series of northward-dipping listric normal faults. These faults are the longest and exhibit the most significant northward displacements within the delta (Hussein and Abd-Allah 2001). Movements along these fault planes are the primary cause of subsidence and sinking of the African margin in the study area.

The east–west trending faults that define the Nile Delta's Hinge Zone change their trend to a north–south orientation in the west (Hussein and Abd-Allah 2001). Interestingly, some faults only deform the Oligocene-Pliocene rocks overlying the pre-Eocene rocks, while others affect the Eocene rocks.

It is essential to highlight that existing seismotectonic models (e.g. Sawires et al. 2015) for Egypt exclude the Nile Delta and Hinge Zone due to a lack of prior seismic activity; however, the 2020 earthquake necessitates a reevaluation of this area's seismotectonic behavior for seismic risk assessment and mitigation.

3 Seismicity of the Nile *Delta*

Egypt's seismic activity varies across the country, with generally moderate activity except for the eastern and northern borders (Fig. 1b). As the figure shows, most of strong earthquakes are reported in the north, along the northern Nile Delta and continental margin, and in the east, along the Red Sea and its gulfs—Suez and Aqaba (Abd El-Aal et al. 2019). Seismic activity in the other parts of the country ranges from negligible to low and diffuse activity. Egypt's seismicity is mainly caused by the Red Sea rifting, DSFS, and recent tectonic activity in the eastern Mediterranean (Abd El-Aal et al. 2019; Ali and Badreldin 2019). Figure 1b highlights that the central Nile Delta region, where the studied earthquake occurred, lacked any recorded seismic activity prior to this earthquake under investigation (22 November 2020).

In recent decades, efforts have been directed towards to understanding seismic near urban centers in Egypt. For this study, we developed a seismicity map considering the NRIAG earthquake bulletin and the recently compiled and revised NRIAG historical earthquake catalog from various sources in 2010 (e.g. Ambraseys et al 1994; Badawy 1999). Figure 1b illustrates that no historical earthquakes are reported in the Nile Delta region in general, nor in the vicinity of the November 22, 2020 earthquake. However, some studies (e.g.Rashwan et al. 2021; Sawires et al. 2015), that did not adopt the NRIAG historical earthquake catalog, depicted historical earthquakes near the location of the 2020 Hinge Zone earthquake.

However, the recent earthquake and reports of some historical activity near the epicentral location raise concerns about future seismic events in the Nile Delta. This highlights a critical question that warrants further investigation: Should the Nile Delta be reclassified as a seismically active zone?

4 Earthquake data and methodology

Studying the focal mechanisms of small earthquakes that are happening for the first time in a region is particularly important for seismic hazard assessment, geodynamics, and risk mitigation for several reasons: 1) They may indicate new fault structures and strain accumulation that were previously unrecognized in

an area; 2) Areas with low background seismicity that then start to experience small quakes may signal a change in regional stresses and upcoming seismic risk that was not accounted for; 3) Rare small events may reflect complex fault interactions, unseen structures, that require further study to understand their implications; 4) The locations, depths, and types of first-time quakes contribute data to improve geodynamic and seismotectonic models; 5) For risk analysis, first-time activity drives updates to seismic hazard maps and preparation for the possibility of larger triggered earthquakes based on scenario-based approach.

It is worth noting that the seismic event occurred in an area characterized by a high population density and extensive agricultural activities, with no quarry-mining operations in the vicinity. In order to differentiate between tectonic and artificial causes, various discrimination techniques, such as spectral analyses, have been regularly employed (Korrat et al. 2022; Korrat et al. 2023). These techniques have been instrumental in excluding alternative mechanisms and providing a clearer understanding of the earthquake's tectonic origin.

In this work, we studied and investigated the source and focal mechanism parameters of the earthquake of 22nd November 2020. This earthquake was recorded by several local seismic stations, both weak and strong motion networks. Several regional seismic networks also captured it (see Appendix A, Table 4). The extracted waveform data from the earthquake is used to estimate the local magnitude, location, fault plane parameters (strike, dip, rake), and kinematic source parameters.

We employed the HYPOINVERSE software (Eaton 1970; Lee and Lahr 1972; Lahr 1980) within the Atlas software suite to estimate the epicentral location and magnitude of the Nile Delta earthquake that occurred on November 22, 2020. This software utilizes the time difference between the first-arriving P and S waves to determine the epicentral location. Additionally, it estimates both local magnitude (ML) and coda wave magnitude (MD) by analyzing amplitude and coda duration.

To refine the initial location determined by the Egyptian National Seismic Network (ENSN), we employed the El-Hadidy (1995) 1D crustal model. This model incorporates local geological characteristics and seismic velocity data specific to the region, leading to a more accurate relocation of the epicenter and magnitude. Also, to re-evaluate the magnitude of the Nile Delta earthquake, we adopted the local magnitude (ML) formula developed for Upper Egypt by Abdullah et al. (2022).

The crustal velocity model, initially developed by El-Hadidy in 1995 for the northeastern part of Egypt, was utilized in this study to estimate the earthquake's hypocenter. Despite the lack of a dedicated model for the Nile Delta region, extensive sensitivity tests were conducted using various models. Through rigorous evaluation, it was determined that El-Hadidy's model consistently yielded earthquake locations with minimal errors in both horizontal and vertical dimensions.

Understanding source characteristics of seismic events is crucial for unraveling the ongoing tectonic processes and earthquake generation, particularly in regions with concealed faults (blind faults). The November 2020 Nile Delta earthquake represents the first event in this area with instrumental recordings since the establishment of the Egyptian National Seismic Network (ENSN) in 1989. Consequently, no prior focal mechanism solutions exist for this region. This study analyzes the earthquake's seismic data, including P and SH wave displacement spectra, to investigate the event's source parameters.

4.1 Focal mechanism analysis

The results obtained from focal mechanism analysis are commonly utilized to determine the slip direction and the stress that caused it on the fault plane. This information helps define the motion directions of lithospheric plates and the stress patterns at earthquake foci, providing an instantaneous depiction of tectonic movements in the area. In this study, we estimated the fault plane solution for the November 22, 2020, earthquake using P wave first motion data from 19 velocity and acceleration stations to ensure good coverage and minimize azimuthal gaps. However, we could not include more stations far from the earthquake's epicenter due to the relatively small magnitude of the analyzed earthquake (ML 3.3).

In this study, we utilized two software packages: PMAN and FOCMEC developed by Suetsugu (1998) and Snoke et al. (2003), respectively. Both packages, written in Fortran, are used to estimate fault plane solutions for relatively small earthquakes ($M < 4$), while full waveform inversion is preferred for more significant earthquakes (Hofstetter 2014). These two

software packages require inputs including the earthquake hypocenter, a set of stations, and the velocity model of El-Hadidy (1995). Suetsugu's package consists of three principal codes: TANGLE, which constructs a travel time table and calculates depth and emergent angles based on the crustal model of the source area; AZMTAK, which prepares the polarity data file containing compression or dilation, take-off angle, and azimuth; and PMAN, which plots the output file in a lower hemisphere projection as shown in Sect. 5. Alternatively, these steps can be omitted by using the azimuths and take-off angles generated by the Hypoinverse earthquake location program (Klein 2002), along with the polarity data of P-waves picked from the vertical component, as input for the PMAN program (Table 1, and Appendix A, Table 1).

The FOCMEC package also includes several programs for constructing and plotting mechanism solutions. These programs utilize input parameters including station sets, azimuths, take-off angles at the source, polarities, and amplitude ratios from P, SV, and SH arrivals. For instance, the program Fileprep prepares the FOCMEC input file using the iasp91 (Kennett and EngdahlE 1991) model to obtain travel times and takeoff angles. Seismic waveform data analysis is performed using the Seismic Analysis Code (SAC) (Goldstein and Snoke 2005), which rotates the horizontal components into transverse and radial components to obtain SH and SV waves. The FOCMEC program outputs all acceptable solutions, imposing selection criteria such as allowing up to two errors for polarity and none for amplitude ratios. The maximum number of solutions is set to 20, with a maximum log10 ratio of 0.1 and lower bounds of 0.05 and 0.15 for P and S radiation factors respectively, while VP/VS is set to 1.732 corresponding to iasp91 (Kennett and EngdahlE 1991) model. In the FOCMEC package, polarities are indicated by directions relative to an observer facing the station with their back to the epicenter. The first motion of the P arrival is either up or down, while the SH arrival is either left or right, and the SV arrival is either upward or backward.

To obtain the faulting mechanism solution the 1D crustal model developed by El-Hadidy in 1995 was also adopted. Each station was carefully selected based on specific criteria, including its ability to provide clear P-wave polarity and have a high signal-to-noise ratio. Furthermore, amplitude ratio analysis was used as an additional tool to validate the results obtained from polarity analysis. The consistency between the outputs of these two methods confirms the accuracy of the faulting mechanism determinations.

4.2 Kinematic source analysis

In this work, the P and SH waves source displacement spectra were analyzed for low-frequency spectral level (flat part, Ω) and corner frequency (f_c) of the Nile Delta's earthquake waveform using the standard Brune's model (Brune 1970 and Brune 1971). The waveform data used in source parameters estimation were recorded by the velocity stations that are located at epicentral distances varying between 16 and 240km (see seismic waveforms shown in Fig. 2 and geographic distribution of the nine stations in Figs. 1b).

In the current analysis, we relied on seismograms recorded by the ENSN seismograph network. ENSN seismic stations are located on rock sites and as far away from anthropogenic activities as possible. Therefore, we believe that relying on vertical component data from stations installed on rock sites effectively mitigates site effect-related modifications. However, strong motion data are inherently affected by site effects because strong motion stations are often deployed on sediment sites. This is one of the reasons why we chose not to use strong motion data in dynamic source characterization.

In this article, we also analyze the spectra of P and SH-wave seismograms for corner frequency and low-frequency spectral amplitude using the standard Brune model (Brune 1970). Rotating the horizontal components to SH wave polarization allows for a more accurate analysis of the shear wave characteristics. Also, this helps reduce interference from P-waves and other seismic phases.

The selection of earthquake waveform dataset follows some criteria: most calibrated seismic stations; most clear digital waveform and the onset of P- and S-wave arrival, located at different epicentral distances and azimuths, signals are not clipped and had good quality and signal-to-noise ratio ($SNR \geq 5$) to do reliable spectral analysis following the threshold recommended by Süle and Wéber (2013); Korrat et al. (2022). The ObsPy Python code was written to calculate the SNR value taking the ratio of the root mean

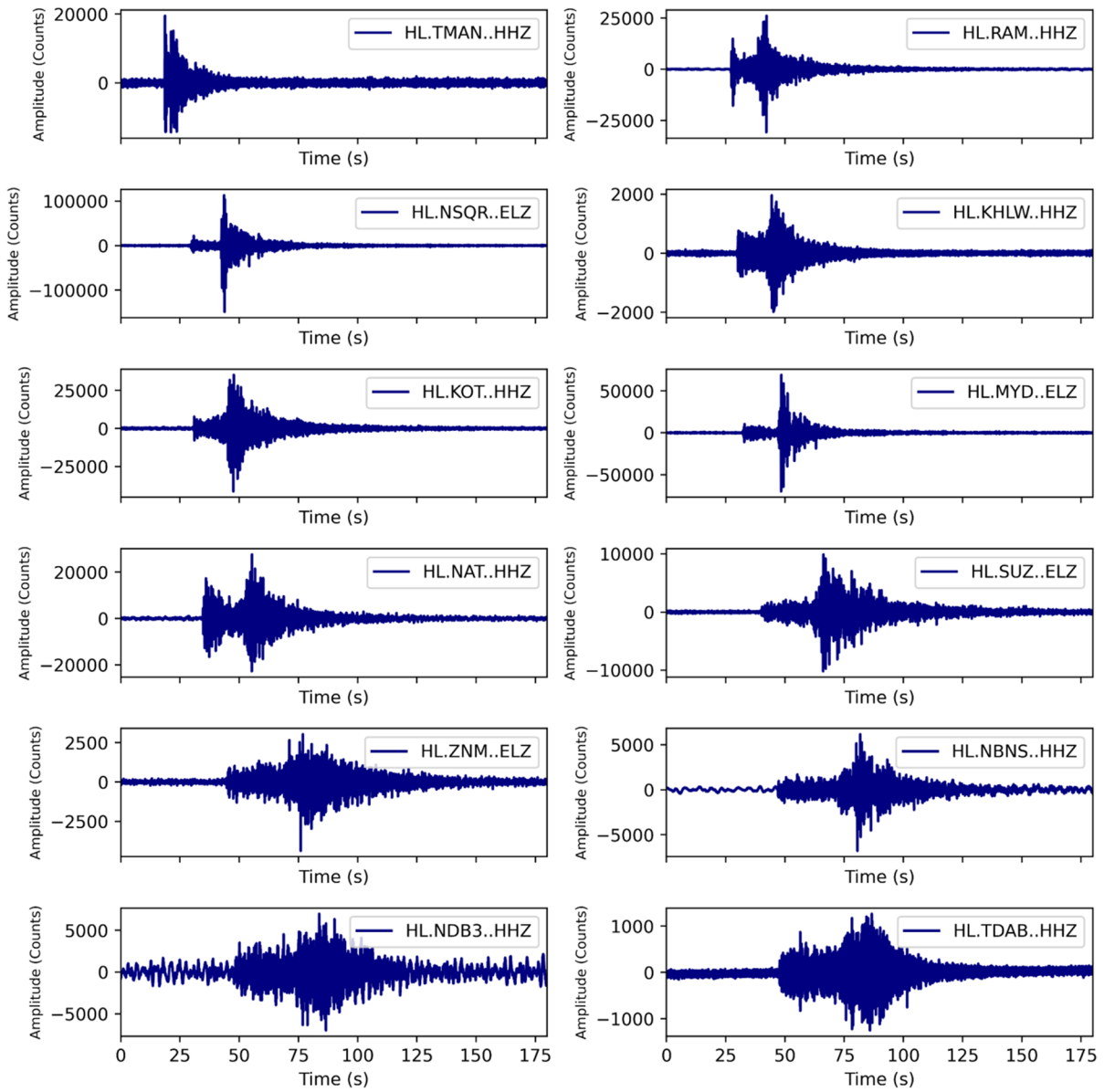

Fig. 2 Seismic waveforms of the Hinge Zone earthquake recorded by both strong motion stations and seismometers operated by NRIAG, as illustrated in Fig. 1b

square (RMS) of the windowed signal for P and S waves to the RMS of the noise signal within the same window size.

Moreover, the selected stations in the dataset were recorded using various types of seismometers (Table 1). Specifically: a) Short-period stations use three-component SS-1; b) Ranger and L4C seismometers with a 1 Hz natural frequency; c) Broadband stations utilize three-component Streckeisen STS-2 seismometers with Trillium 120-s periods; d) The SUZ station has only one vertical component.

The EQK_SRC_PARA software (Kumar et al. 2012) is employed for analyzing seismic data. It calculates P-wave displacement Fourier spectra from vertical component seismograms and SH-wave displacement spectra from the rotation of horizontal component seismograms, considering the station azimuth value.

The spectral analysis involved measuring the low-frequency spectral level of P and SH waves displacement spectra (Ω_P and Ω_S) and corner frequencies fc_P and fc_S observed at the recording stations. The measured values (i.e., Ω and fc) are used to determine source parameters following omega-square Brune's source model. To perform the spectral analysis on earthquake waveforms using the Fast Fourier Transform (FFT), the first step in the signal pre-processing is to remove the mean and linear trends. In the second step, the instrumental response effect was firstly eliminated for each recorded station by deconvolution of the system transfer functions, which were calculated using poles, zeros values, and other system information. Consequently, the seismograms were transformed into velocity waveforms (transformed from original counts to cm/sec). After instrumental correction, the calculated P and SH wave displacement spectrum $D(R,f)$ recorded at the station at an epicentral distance R (source to the station) and for frequency f can be described as (Garcia-Garcia et al. 1996):

$$D(R,f) = G(R)\ .\ A(f,t).\ S(f) \tag{1}$$

where t is travel time, $G(R)$ stands for geometrical spreading, $A(f,t)$ is anelastic attenuation, and $S(f)$ is the amplitude source spectrum. Therefore, The observed spectra $D(R,f)$ must be corrected for geometrical spreading and anelastic attenuation (distance corrections) to estimate the source spectrum $S(f)$. Anelastic attenuation can be divided into two parts as follows (Singh et al. 1982):

$$A(f,t) = P(f)\ .\ L(f) \tag{2}$$

where the first term $P(f) = exp[-\pi ft/Q(f)]$ stands for the propagation path effect that describes the path-dependent attenuation (due to the propagation path of seismic waves from the source to the recorded station), with $Q(f)$ is the frequency-dependent quality factor. The second term $L(f) = exp[-\pi f\kappa]$ is the site effect which describes the near-surface attenuation characterized by the kappa k parameter. It represents spectrum decay, which is largely caused by near-surface crustal effects that absorb amplitudes at high frequencies. However, EQK_SRC_PARA software was modified to allow the estimation of the k factor.

Hence, to retrieve source spectra, the observed P and SH waves displacement spectra are corrected for two effects: (1) frequency-independent geometrical spreading and (2) frequency-dependent anelastic attenuation that includes the path and site effects.

In this study, the geometrical attenuation was corrected based on the formulation suggested by Havskov and Ottemöller (2010), $GS(R) = R - 1$ for $R \leq Ry$ and $GS(R) = (RRy)^{-0.5}$ for $R > Ry$, the value of Ry is the regional dependent and may be taken as twice the thickness of crust (Herrmann and Kijko 1983). Moreover, attenuation has two effects: it changes the spectrum shape, affecting the corner frequency determination and it also changes the low-frequency spectral level, affecting the estimation of the seismic moment (Süle and Wéber 2013; Korrat et al. 2022). Therefore, the correction for attenuation is particularly important to get a reliable corner frequency.

In this study, in order to correct the propagation path-attenuation effect, we have taken into account two attenuation studies that were conducted in our study area. The first approach, by El-Hadidy et al. (2006), estimated the attenuation behavior of coda waves Qc in the vicinity of the Cairo metropolitan area, located a few tens of kilometers south of our study area. They found that $Q_c(f) = 85.68f^{0.79}$. Assuming that Qc is a good approximation of Qs, as emphasized by Kiszely (2000), Baumbach and Bormann (2009), and Süle and Wéber (2013), we can accept that $Qc \approx Qs.Thus, Q_s(f) = 85.68f^{0.79}$ to correct S-wave spectra. Since $Qp(f)$ data is unavailable for our study area, we may use the approximation $Qp \approx 2Qs$, supported by several researchers, e.g. Abercrombie and Leary (1993); Anderson et al. (1965);Barton (2007), and Baumbach and Bormann (2009). Therefore, we derived $Q_p(f) = 171.36f^{0.79}$ for correcting P-wave spectra.

The second, more recent, and most robust attenuation study we relied on to correct the attenuation effect for both P and S-wave spectra is by Abdel-Fattah (2009). Abdel-Fattah (2009) estimated the attenuation of body waves (Qp and Qs) separately in the same study area beneath the vicinity of Cairo metropolitan area (Egypt) using the coda normalization method. The frequency-dependent attenuation approaches were found to be $Q^{-1}p(f) = \left(19x10^{-3}\right)f^{-0.8}$ *and* $Q^{-1}s(f) = \left(7x10^{-3}\right)f^{-0.85}$ for P and S-waves, respectively.

We opted for Abdel-Fattah's (2009) attenuation approach for a couple of reasons: (i) it is the most recent study, utilizing a larger dataset of earthquake records

and stations compared to El-Hadidy et al. (2006). (ii) Abdel-Fattah (2009) established frequency-dependent attenuation approaches for $Qp(f)$ and $Qs(f)$ separately, which is more appropriate for our study for correcting P and S-wave spectra. In contrast, El-Hadidy et al. (2006) only derived $Qc(f)$. Therefore, We derived $Qp(f)$ and $Qs(f)$ from $Qc(f)$ using approximations from other studies above, which can lead to potential ambiguities and uncertainties in the calculations. Longer calculation paths, as in the derivation from El-Hadidy et al. (2006) data, are generally more error-prone than shorter, more direct methods. To improve the accuracy of future studies, we suggest that direct measurements of $Qp(f)$ and $Qs(f)$ be conducted within the study area. This would eliminate the need for approximations and reduce the potential for errors, leading to more precise correction of the P and S-wave spectra.

In addition, the spectra also were corrected for the near-surface attenuation effect that was calculated from the analyzed recorded waveform data of seven stations. After correcting for geometrical and anelastic attenuation, the resulting corrected P or SH waves displacement amplitude source spectrum $Dc(f)$ is compared to Brune's model as given by the following relation (Brune 1970; Hanks and Wyss 1972):

$$Dc(f) = \frac{\Omega o}{(1+\frac{f}{fc})^2} = \frac{M_o R_{\theta\varphi} S_a}{(1+\frac{f}{fc})^2 4\pi\rho v^3 R} \tag{3}$$

Once the corrected displacement spectra were calculated using EQK_SRC_PARA software that performs Brune's source model for spectra from each station that records the event, the spectral parameters including the low-frequency spectral level Ω_0 and the corner frequency f_c at the source were estimated. Considering P and S wave data separately, the seismic moment M_o, fault radius r, displacement d, stress drop $\Delta\sigma$, along the fault, and the moment magnitude Mw can be derived from the P and SH wave displacement spectra following Brune's (1970, 1971), Hanks and Wyss (1972), and Kanamori (1977) relations:

$$M_{o(P,S)} = \frac{4\pi\rho V(P,S)^3 R\Omega_{(P,S)}}{R_{\theta\varphi\,(P,S)} S_a} \tag{4}$$

$$r_{(P,S)} = \frac{K_{(P,S)} V_S}{2\pi f_{c(P,S)}} \tag{5}$$

$$d_{(P,S)} = \frac{M_o}{\pi\rho Vs^2 r^2} \tag{6}$$

$$\Delta\sigma_{(P,S)} = \frac{7M_o}{16r^3} \tag{7}$$

$$M_W = \frac{2}{3}\log(M_o) - 10.7 \tag{8}$$

where ρ is the density, v is the velocity ($v_p or v_s$) that are picked from El-Hadidy (1995) velocity model that was used for event hypocentral location, R is the epicentral distance, S_a is the free surface effect (assumed to be 2), and $K_P = 3.36$, $K_S = 2.34$. In these calculations, the average values are used of radiation pattern coefficients $R_p(\theta,\varphi)$=0.52 for P waves and $R_s(\theta,\varphi)$ =0.55 for S-waves (Boore and Boatwright 1984). The average values of delta earthquake source parameters, as well as their standard deviations from P and SH wave spectra, are determined independently using the equations presented by Archuleta et al. (1982):

$$x_{avg} = \text{anti log}\left(\frac{1}{N}\sum_{i=1}^{N} logx_i\right) \tag{9}$$

where N denotes the number of stations where an event has been recorded. The variance of the individual logarithmic values is used to compute the standard deviations (SD) of the source parameters (x= M_o, r, d, and Mw) using the following equation:

$$\text{SD}\left[logx_{avg}\right] = \left[\frac{1}{N-1}\sum_{i=1}^{N}(logx_i - logx_{avg})^2\right]^{1/2} \tag{10}$$

5 Results and discussion

The waveform data from ENSN were adopted to determine the earthquake's hypocenter, origin time and magnitude (as presented in Table 1). We estimated the epicenter by analyzing the arrival times of P and S waves at various seismic stations. To minimize the azimuthal gap (uneven distribution of stations around the epicentre), data from additional regional networks were incorporated.

High-accuracy earthquake parameters were achieved through careful manual phase picking and applying a suitable crustal structure specific to the

region (details in Table 1). This crustal model and the increased number of seismic stations contributed to reducing the horizontal error (epicentral distance uncertainty) and vertical error (depth uncertainty) to 0.8 km and 1.6 km, respectively (Table 1).

In this study, we adopted the local magnitude (ML) formula developed for Upper Egypt by Abdullah et al. (2022) to reappraisal the size of the Nile Delta earthquake. This formula incorporates corrections to the Richter ML scale to take into account the difference in seismic wave attenuation between southern Egypt and southern California.

It is worth noting that the ML is calculated using the maximum of half peak-to-trough amplitude of either the Sg or Lg phase from the two horizontal components recorded by closest seismic stations. These amplitudes are first deconvolved from the instrument response and then convolved with the response of the Wood-Anderson seismograph to simulate its output. Consequently, the average earthquake magnitude determined using Abdullah et al. (2022) formula is (ML 3.3). The main results of this study are as follows:

5.1 Focal mechanism solutions

A comprehensive analysis of P and S wave polarities and amplitude ratio for the studied earthquake allowed us to infer the style, potential orientations and motion of the causative fault. The obtained fault plane solutions from the two approaches shown in Sect. 4 provide a reasonably well-constrained result, indicating an oblique-slip faulting mechanism along the E-W and NNW-SSE nodal planes (Fig. 3, Table 2). Also, hereinafter we provide a comparative analysis for the 2020 Hinge Zone earthquake with focal mechanism catalogue of earthquakes occurred in the study region. This can help to gain valuable insights into the seismotectonic framework of the studied region. This

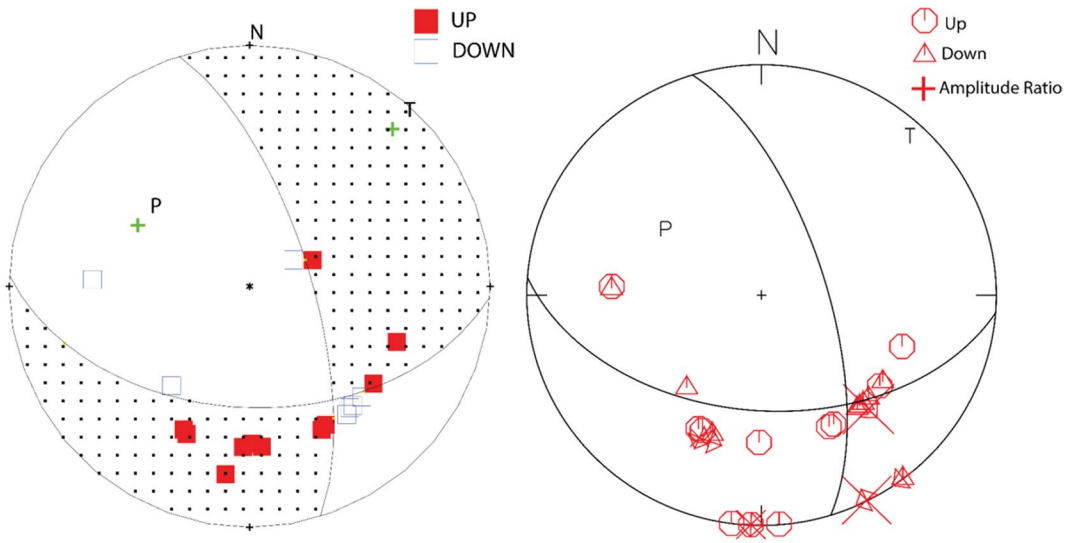

Fig. 3 Shows the focal mechanism solution produced by PMAN (left panel) and one selected solution from the six acceptable solutions generated by FOCMEC (right panel) (refer to Table 2 for focal mechanism parameters)

Table 2 Focal mechanism solutions of the 2020 Hinge Zone earthquake using PMAN and FOCMEC softwares

Date DD/MM/YY	Nodal plane 1			Nodal plane 2			P -axis		T -axis		Approach
	Strike	Dip	Rake	Strike	Dip	Rake	Az	Pl	Az	Pl	
22/11/2020	341°	69°	-47°	92°	46 °	-151°	296°	47.0°	41.0°	14.0°	PMAN
	342.86 °	67.48 °	-45.90 °	94.43°	48.44 °	-149.21 °	299.87 °	47.73°	42.73 °	11.44 °	FOCMEC

framework essentially describes the link between the regional tectonics (plate movements, faults) and the resulting earthquake activity.

Figure 3 illustrates the focal mechanism solutions for Hinge Zone earthquake, presented in a lower hemisphere projection of the focal sphere using two approaches. The left panel of Fig. 3 is the initial solution obtained from PMAN, utilizing the P wave polarity onset dataset as discussed in Sect. 4.1.

The right panel depicts the final solution derived from FOCMEC, which incorporates additional or constraining information of SV, SH, polarities, and SH/P and SV/SH amplitude ratios.

The absence of aftershocks and prior fault plane solutions in the earthquake zone hinders definitive identification of the main causative fault with high confidence. However, by integrating the available surface and subsurface structural maps (comprehensively discussed in Sect. 2) with the established structural framework of surrounding areas (e.g., Shalaby and Sarhan 2021, 2023), particularly the CSSZ and the Hinge Zone, we favor an east–west trending normal fault with a subordinate component of dextral motion as the most likely source of the earthquake.

As discussed earlier (Sect. 2), these nodal planes orientations are commonly observed and mapped in the subsurface along the eastern region of the Tethys Trend /Hinge Zone (Sarhan et al. 2014). Geophysical studies across this zone reveal no considerable variations in crustal types (Saleh 2012). However, it is a critical structural boundary separating the African continental crust from its stretched-thin passive margin (Shalaby and Sarhan 2023).

Furthermore, the similar nodal plane orientations are prominent in surface geological mapping of the CSSZ, as it represents the southern marginal shear boundary of the Nile Delta cone (e.g. Hussein and Abd-Allah 2001; Hammam et al. 2020). It demarcates the transition between the uplifted Eocene plateau to the south and the northern plain dominated by deltaic sedimentary facies. It's important to note that both the Tethys Trend/Hinge Zone and the CSSZ trend east–west, traversing the central and southern portions of the Nile Delta cone, respectively. Additionally, both zones exhibit subordinate populations of northwest-southeast trending lineaments, particularly within the CSSZ (e.g., Hussein and Abd-Allah 2001; Sarhan et al. 2014).

The distribution pattern of fault mechanism solutions, as illustrated in Fig. 4, offers significant insights into the seismic activity of the studied region. Figure 4 provides a comprehensive overview that can guide us assess whether the Nile Delta earthquake originated from the same fault system or a distinct fault segment. This analysis also sheds light on the regional tectonic setting, which is crucial for characterizing earthquake sources and their associated parameters. Consequently, this information contributes to a deeper understanding of seismic sources and has a direct application in seismic source and ground motion modeling.

As a comparative analysis, the faulting mechanism of the 2020 Nile Delta earthquake is compared with those of events that occurred along the CSSZ (i.e., 29th June 2000, ML 4; 07th July 2005, ML 4.2, and 30th October 2007, ML 3.7). As reported by Abou Elenean et al. (2010), the focal mechanism solutions for these prior CSSZ earthquakes exhibited primarily normal faulting with a minor strike-slip component (oblique mechanism) along northwest-southeast and east–west nodal planes (Fig. 4).

A comparison with the mechanism of the October 12th, 1992 Cairo earthquake (mb = 5.8) reveals consistency between the P and T axes with the current solution for the 2020 Nile Delta earthquake. The focal mechanism solutions of earthquakes occurred in Northern Egypt, along with a the 2020 Nile Delta earthquake is an indication that they exhibit a consistent faulting pattern as shown in Fig. 4. These observations support the hypothesis that pre-existing east–west and northwest-southeast trending faults are being reactivated due to partial transfer of rifting deformation from the Red Sea-Gulf of Suez region. Notably, most of the analyzed mechanisms indicate either pure normal faulting or an oblique sense of normal faulting with a subordinate right-shear component. The focal mechanisms of DSZ and CSSZ (adopted from Ali and Badreldin 2019; Badreldin et al. 2019) exhibit similarities, as both zones are part of the major east–west trending transcurrent shear system located north of the Gulf of Suez rift. However, these zones show distinct faulting mechanisms. However, the fault plane solutions in DSZ indicate a dextral strike-slip faulting mechanism with a minor normal component (Abou Elenean 1997; Ali Sherif 2011). In contrast, the CSSZ is characterized by

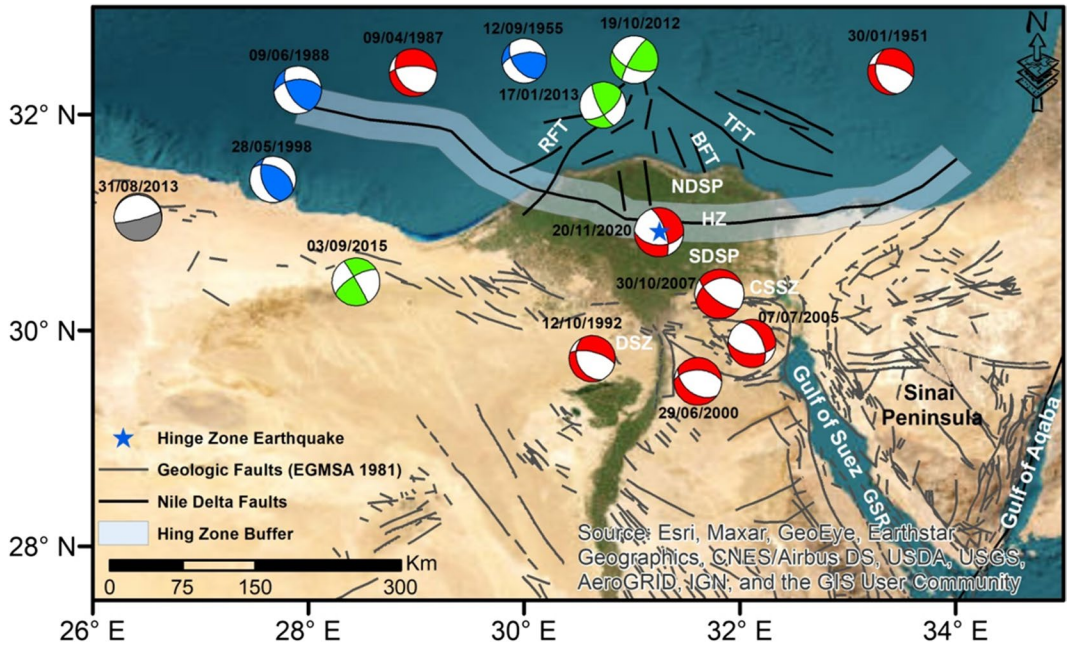

Fig. 4 Regional tectonic map, showing the major tectonic plate boundaries and their kinematics. White arrows show the stress regime and plate boundaries kinematic interactions. Spatial distribution of the fault plane solutions of significant earthquakes that occurred in north Egypt compiled from recent publications and the studied earthquake (marked by a blue star at the center of the beach ball) adopted from Korrat et al. (2005); Abou Elenean et al. (2010); Abu El Nader et al. (2013); Abd El-Aal et al. (2017); Badreldin et al. (2019). GSR: Gulf of Suez Rift, CSSZ: Cairo Suez Shear Zone, DSZ: Dahshour Seismic Zone, NDSP: North Delta Structural Province, SDSP: Southern Delta Structural Province, HZ: Nile Delta's Hinge Zone, RFT: Rosetta fault trend, TFT: Temsah fault trend, and BFT: Bardawil Fault Trend)

normal faulting with a subordinate strike-slip component (Ali and Badreldin 2019; Badreldin et al. 2019; Abou Elenean and Hussein 2008). This significant shift in the dominant type of shear motion from west to east along the two zones is likely a mechanism to accommodate the ongoing extension in the Gulf of Suez rift region. Furthermore, an analysis of the combined focal mechanism solutions for the region (Fig. 4) suggests a variation in the direction of crustal extension from northeast to north-northeast-south-southwest directions on the NW- and E-W trending normal and strike-slip faults (Moustafa and Abd-Allah 1992), respectively.

The northward dipping listric normal faults in the Hinge Zone strike generally in the east–west direction in the eastern region of the Nile Delta (Sarhan et al. 2014; Shalaby and Sarhan 2023); oriented parallel to the common orientation of the CSSZ. However, these faults progressively change strike to north–south further westward (Hussein and Abd-Allah 2001). This shift in fault orientation suggests northeast-facing, bowl-shaped basin geometry. This geometry or pattern of normal faults may explain the observed thickening of the deltaic sedimentary sequence towards the northeast and the potential for northeastward gravitational collapse of the delta sediments due to extension in that direction (Shalaby and Sarhan 2023). Furthermore, southward dipping normal faults recorded in the focal mechanism solution of the 2020 HZ earthquake are typically considered as the antithetic faded trend of the conjugate array of the common shallow northward listric faults. Sarhan et al. (2014) matched these antithetic arrays on seismic lines transecting the Nile Delta Hinge Zone area. Therefore, the current focal mechanism solution is similar to the transtentional deformation of the southern CSSZ that is principally constrained by east–west trending normal faulting with slight dextral strike-slip of motion.

The northern African continental margin in Egypt consists of the Nile Delta cone, bordered to the west by the northeast-southwest trending Rosetta Fault System (RFT) (Segev et al. 2018; Shalaby and

Sarhan 2023) and to the east by the northwest-southeast trending Tethyan Fault Zone (TFZ) (Mascle et al. 2000; Loncke et al. 2006). The RFZ represents the common margin of Levant and Herodotus basins in the Eastern Mediterranean Sea region (Hussein and Abd-Allah 2001; Jagger et al. 2018). Notably, this fault is full-exposed along the western margin of the Eratosthenes Seamount (ESM) (Rybakov et al. 2008; Abd-Allah et al. 2012; Skiple et al. 2012), where it forms a prominent submarine fault scarp (Shalaby and Sarhan 2023). Bathymetric data (e.g., Loncke et al. 2006) reveal clear evidence for reactivation of the RFZ offshore between the Nile Delta slope and the ESM. This reactivation is manifested by deformations in the Messinian salts and overlying sediments, suggesting the RFZ played a role in channeling Messinian salt movement towards the Herodotus and Levant basins (Shalaby and Sarhan 2023).

Based on the available evidence, we propose that the RFZ remains tectonically active, particularly along the western margin of the ESM and offshore from the Nile Delta cone. The focal mechanism solution for an earthquake offshore of the Nile Delta along the RFZ (beach ball labeled 17/01/2013 in Fig. 4) indicates dominant strike-slip faulting with some thrusting component, suggesting crustal shortening in a west-northwest-east-southeast direction. This trend of shortening is likely causing the RFZ to dextrally offset the Crete-Cyprus thrust belt, particularly near Cyprus.

Further northeast, along the southern margin of the TFZ, the focal mechanism solution from 2012 (Fig. 4) exhibits a predominantly strike-slip faulting pattern with minor reverse motion components. This indicates a horizontal compression in the north-northwest-south-southeast direction, which is consistent with the regional far-field stress at the Crete-Cyprus thrust belt, characterized by bulk horizontal compression in the north–south direction (Moustafa et al. 2022). This orientation of crustal shortening across the NW-trending TFZ originates a wide zone (more than 20 km width) of dextral shearing along the northern and northeastern fringes of the Nile Delta cone (Shalaby and Sarhan 2023).

Figure 4 reveals contrasting focal mechanism solutions for earthquakes in the region. The 1951 and 1987 events exhibit normal faulting, while the 1955 and 1988 events show reverse faulting. These contrasting solutions highlight the present-day compressional stresses resulting from the convergence of the African and Eurasian plates. We attribute these variations to the irregular geometry of the Crete-Cyprus thrust belt, which primarily induces bulk crustal shortening in the north–south (N-S) direction and complementary extension in the east–west (E-W) direction (Shalaby and Sarhan 2021). South of the thrust belt, the submerged Mediterranean Ridge (associated with the foreland belt) has inverted the African margin through back-thrusting, reactivating the African passive margin with reverse faulting.

Near Ras El Hekma in the Western Desert, compressional horizontal stress is observed due to a vertical fault trending (fault plane solution of the 28/05/1998 earthquake) in the ENE-WSW direction, consistent with E-W trending tensile fractures commonly associated with crustal extension in the N-S direction. The tectonic origin of this tensile stress remains unclear but may be related to the vertical arching of the continental passive margin at shallow depthsas a result of crustal shortening in the northwest-southeast (NW–SE) direction at deeper levels (Shalaby and Sarhan 2021).

The Eastern Mediterranean and the Nile Delta Hinge Zone are intricately linked through a complex network of tectonic processes, fault systems, and plate interactions. This intricate relationship defines the geological and seismic characteristics of both regions, making them a crucial area of study for understanding regional tectonics. Analysis of seismic data suggests the Temsah, Rosetta, and east–west trending faults within the Nile Delta Hinge Zone originated during the Early Oligocene epoch and were reactivated multiple times throughout later periods (Hussein and Abd-Allah 2001). Interestingly, the structural features and deformations observed offshore closely resemble those found in the Hinge Zone itself. Two primary mechanisms are thought to be responsible for the deformation of the Nile Delta Hinge Zone: 1- **Late Oligocene-Early Miocene Compression:** This period witnessed a northwest-southeast to north-northwest-southeast directed compressional event. This compression reactivated pre-existing east–west trending faults, evident from their upward extension through Eocene and older rocks and their influence on younger Oligocene-Pliocene formations; 2- **Northward Gravitational Sliding:** The weight of the Oligocene-Pliocene shale and sandstone formations is believed to have caused them to slide northward over

the underlying Eocene carbonate rocks. These two mechanisms likely acted in conjunction to shape the deformation of the Nile Delta Hinge Zone.

The focal mechanisms described above reveal contrasting tectonic regimes of the Nile Delta offshore and its inland fault zones. Two possible scenarios can explain these complicated structural settings: (1) the differences in local stress regimes due to variations in crustal thicknesses that altered the vertical stress axes, inland along the Hinge Zone and the CSSZ region and surroundings. The maximum principle stress axis tends to be in a sub-vertical attitude: this resulted in prevalence normal faulting. In contrast, the Nile Delta offshore focal mechanisms are characterized by regions of thinned continental crust that relatively reduces the vertical stress; as a result the intermediate principle stress axis tends to be sub-vertical that derives predominance strike-slip motions. (2) Shalaby and Sarhan (2023), and many references therein, presented some evidence that the subduction of the Levant basin had ceased along the Cyprus-Crete thrust belt, possibly due to approaching the ESM, the more buoyant continental block, to the Crete belt. Accordingly, with ongoing approaching Africa to Eurasia, the deformation on the thinned crust of North Africa might be accommodated by up-arching, leading to shallow crustal stretching in the N-S direction. Thus the inland E-W trending fault zones against the Levant basin are predominantly characterized by normal faulting along discrete fault zones in the Nile Delta Hinge zone and CSSZ. In contrast, horizontal shortening along the Nile Delta offshore due to its proximity to the Cyprus-Crete belt results in predominance of strike-slip deformations with some components of reverse faulting.

5.2 Kinematic source parameters

In accordance with the source model (Brune 1970, 1971), the kinematic source parameters of the Delta earthquake have been estimated. Figure 5 shows the processing and analysis of the displacement spectra at selected seismic stations. The analyzed time windows of the P and SH waves are marked by highlighted green rectangles. The best-fitting theoretical Brune's source spectral model is marked by a blue curve (Fig. 5). The obtained spectral parameters Ω and f_c are given for each Brune's spectrum. The estimated source parameters for each station (M_o, r, Mw, d, and $\Delta\sigma$) are also given. The results show that the corner frequencies fc(P) and fc(S) values are in the range of 5.56–7.53Hz with an average value of 6.32 Hz (SD ± 0.10) and 4.13–5.51Hz with an average value of 4.93 Hz (SD ± 0.11), respectively, and fc(P) is basically larger than fc(S), with an average ratio of 1.28. Similar results of the fc(P) > fc(S) ratio was obtained by other authors (Hanks and Wyss 1972; Watanabe et al. 1996; Tusa and Gresta 2008; Korrat et al. 2022). The obtained source parameters also include the obtained seismic moments which vary from 1.24e + 14 to 3.83E + 14 Nm for P-waves with an average value of 1.85E + 14Nm (SD ± 0.37) and from 0.99E + 14 Nm to 4.77E + 14 Nm for S-waves with an average value of 1.87E + 14 Nm (SD ± 0.53). While the average source values of radius and stress drop are calculated to be 322 ± 0.10m (P-wave), 287 ± 0.11m (SH-wave) and 24.35 ± 0.49bar (P-wave) and 34.6 ± 0.26bar (SH-wave), respectively and the relative displacements calculated from P and SH wave are 1.31 ± 0.43 and 1.67 ± 0.34cm, respectively (Table 3). The obtained *k* values were found between 0.021 and 0.044s with a mean of 0.03 ± 0.009s for P waves and between 0.018 and 0.063s with a mean of 0.02 ± 0.017s for SH waves, which is relatively greater than that of Abou Elenean et al. (2010). They found the value of the *K* parameter ranges from 0.01–0.03 at the surface for P-wave. The estimated stress drop value is relatively agreed with that of other works corresponding to inland areas (e.g. Abou Elenean et al. 2010). The main results are shown in Fig. 5 and summarized in Table 3. These results could be used to improve understanding of contemporary seismotectonic processes and can contribute to an evaluation of potential seismic hazard.

6 Summary and conclusions

The Nile Delta is in close proximity to three major active tectonic plate boundaries as discussed in Sect. 2. The major source of ongoing tectonic deformation is remote and took place along the aforementioned mentioned margins as shown by an observed highest rate of seismic activity. Meanwhile, a part of that deformation is transferred to the land to rejuvenate some of the pre-existing NW–SE, WNW–ESE, E–W and WSW–ENE faults with predominant normal faulting with slight shear component (Abou Elenean et al. 2010).

The earthquake occurred on 22nd November 2020 (Mw 3.5), in the Nile Delta, Northern Egypt is

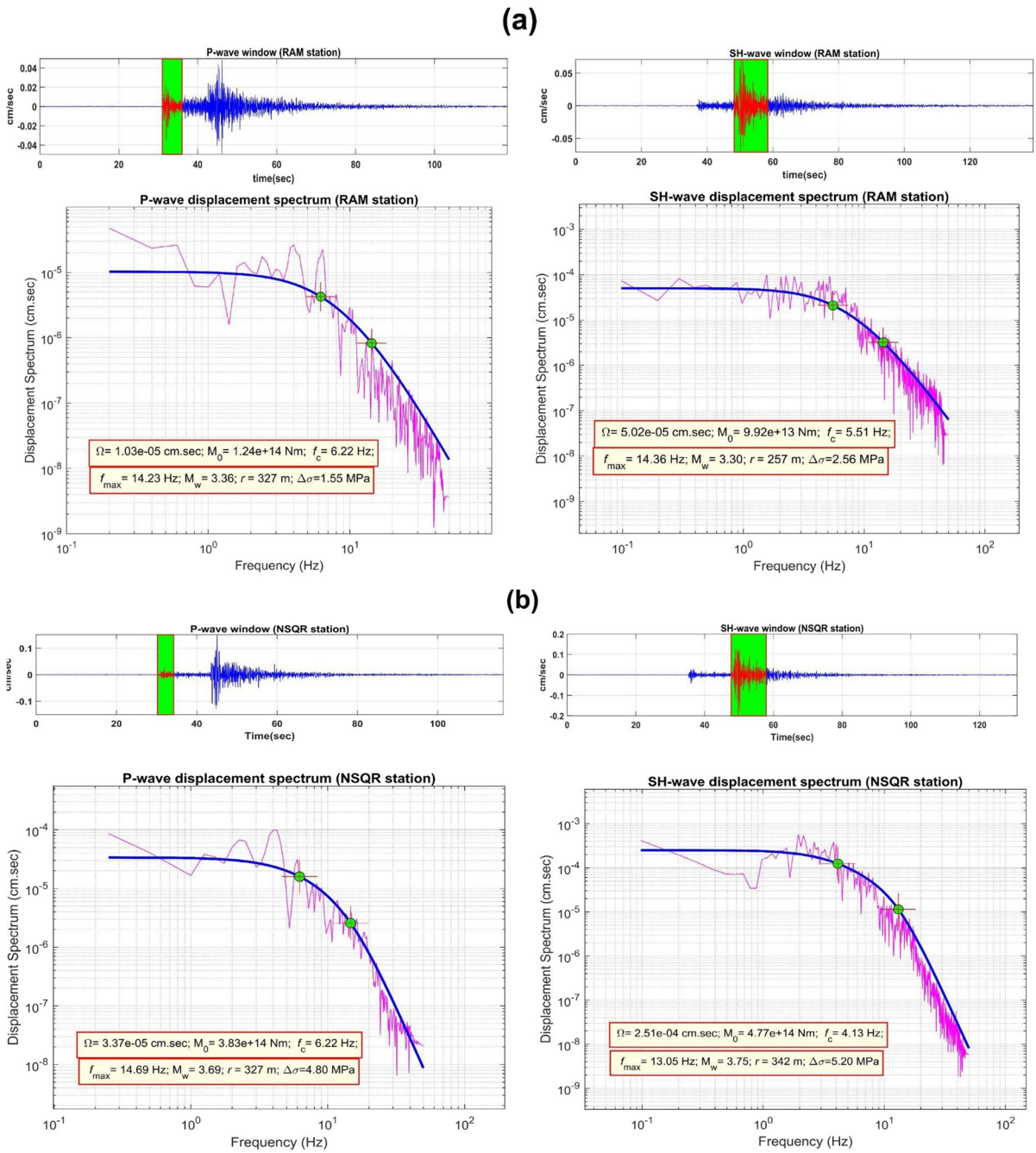

Fig. 5 Vertical and SH component velocity seismograms of the Hinge Zone earthquake and their corrected P- and SH-wave displacement spectra that calculated from four seismic stations; (**a**) RAM station that is located at 97.6 km from the epicenter, (**b**) NSQR station (Δ = 115km), (**c**) KOT station (Δ = 123km), (**d**) MYD station (Δ = 132km). The analyzed time windows of P- and SH-wave are marked by highlighted green rectangles. The best-fitting theoretical Brune's source spectral model is marked by a blue curve. The obtained spectral parameters Ω and f_c are given for each Brune's spectrum. The estimated source parameters for each station (M_o, r, Mw, d, and Δσ) are also given. F_{max} represents the maximum cut-off frequency at which the spectrum decays again rapidly in high frequency

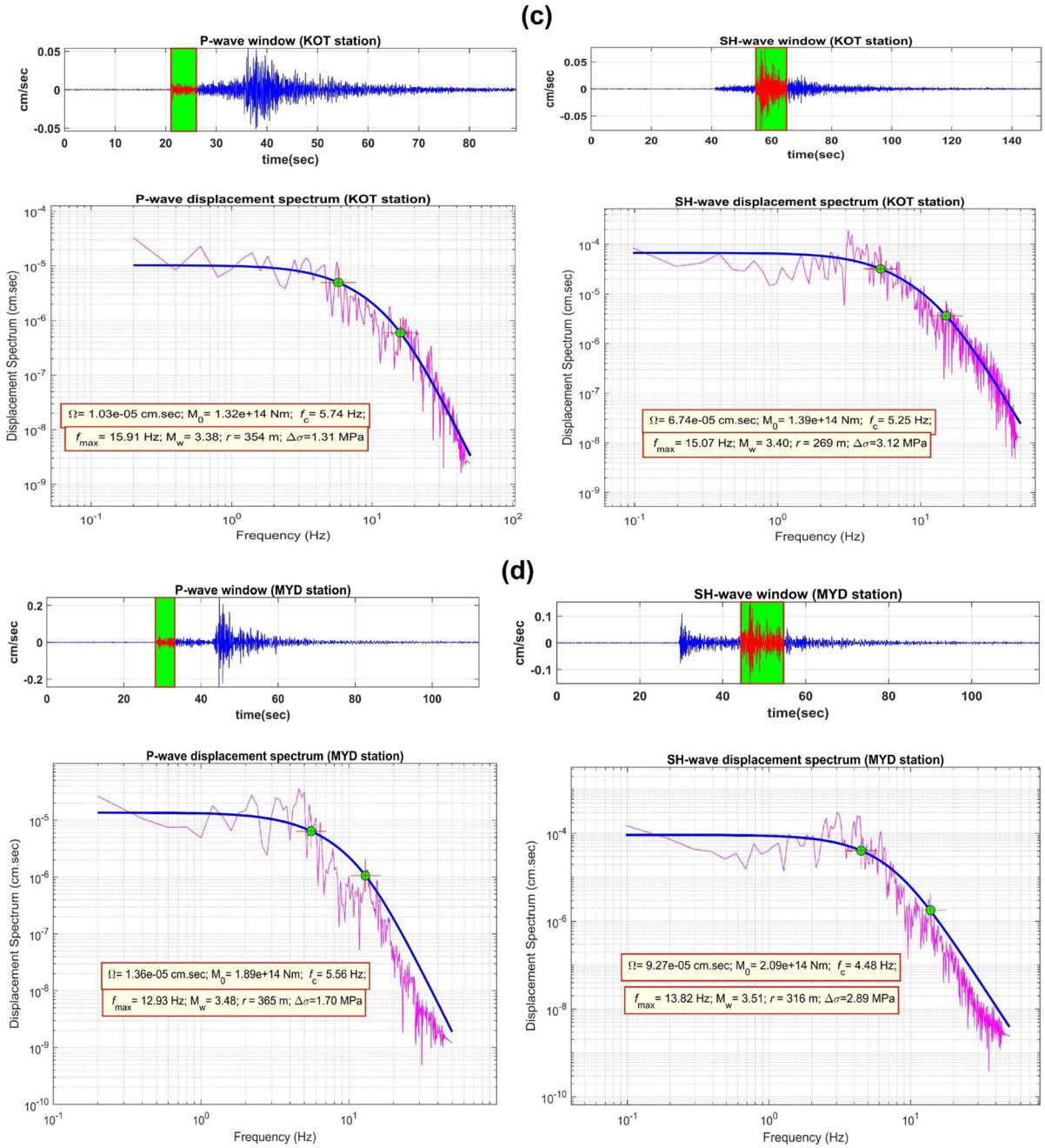

Fig. 5 (continued)

the first ever instrumentally recorded in this region. Furthermore, studying it presents an opportunity to enhance our current understanding of the seismotectonic setting in the Nile Delta region. This earthquake represents a manifestation of the present-day active tectonics in this new seismic source. It was located within the Hinge Zone buffer (Fig. 1), about 16 km from southeast of Mansoura city at a depth of 18 km, as indicated in Sects. 1 and 2.

The mechanism for this earthquake indicates a normal faulting event with a small strike-slip component along the nodal planes of E-W and

Table 3 Estimated source parameter values (M_o, f_c, r, Mw, d and $\Delta\sigma$) with their standard deviations of delta earthquake calculated from P- and SH-wave displacement spectra. Results are given for P and S wave data separately. Unit of stress: 1 bar = 10^5 Pascal (Pa). AV is the average value and SD is the standard deviation

Station Code	Δ(Km)	Az°	Ω(P) (cm.sec)	$\Omega(S_H)$ (cm.sec)	M_o (P) (Nm)	M_o (S_H) (Nm)	f_c(P) (Hz)	f_c (S_H) (Hz)	r (P) (m)	r (S_H) (m)	d (P) (cm)	d (S_H) (cm)	Δσ (P) (bar)	Δσ (S_H) (bar)	M_w (P)	M_w (S_H)
RAM	97.6	142	1.03E-05	5.02E-05	1.24E+14	9.92E+13	6.22	5.51	327	257	0.85	1.1	15.5	25.6	3.36	3.30
NSQR	115	183	3.37E-05	2.51E-04	3.83E+14	4.77E+14	6.22	4.13	327	342	2.63	2.99	48.0	52.0	3.69	3.75
KOT	123	153	1.03E-05	6.74E-05	1.32E+14	1.39E+14	5.74	5.25	354	269	0.77	1.41	13.1	31.2	3.38	3.40
MYD	132	200	1.36E-05	9.27E-05	1.89E+14	2.09E+14	5.56	4.48	365	316	1.04	1.54	17.0	28.9	3.48	3.51
NAT	155.3	204	1.21E-05	6.13E-05	1.94E+14	1.62E+14	6.74	5.17	302	274	1.56	1.59	30.9	34.5	3.49	3.44
ZNM	231.5	137	1.44E-05	4.34E-05	1.72E+14	1.94E+14	7.53	5.18	270	273	1.73	1.91	38.3	41.6	3.46	3.49
SUZ	193	127	9.89E-06	-	1.88E+14	-	6.42	-	316	-	1.38	-	25.9	-	3.48	-
AV			1.35E-05	7.71E-05	1.85E+14	1.87E+14	6.32	4.93	322	287	1.31	1.67	24.35	34.6	3.47	3.48
SD			±0.42	±0.63	±0.37	±0.53	±0.1	±0.11	±0.1	±0.11	±0.43	±0.34	±0.49	±0.26	±0.03	±0.04

NNW-SSE directions, as dicussed in Sect. 5.1. Furthermore, the focal mechanism solution of the 2020 Hinge Zone earthquake indicates southward dipping normal faults. These faults are typically considered to be the lesser developed counterpart (or complementary structure) of the more prominent, northward dipping listric faults commonly found at shallow depths (Sarhan et al. 2014). The current focal mechanism solution for the eastern Nile Delta Hinge Zone aligns with its known geological structure. This structure is dominated by east–west trending normal faulting with a minor component of dextral strike-slip motion, similar to the transtensional deformation observed in the southern CSSZ.

This solution is similar to the source mechanism of the 7 July 2005 earthquake, ML = 4.2 (Abou Elenean et al. 2010) confirms the extension of the Suez Cairo Alexandria trend. The shear transforms the fault zone from the northern Gulf of Suez to the western Delta. The NE-SW of the T-axis indicated by the mechanism of this event agrees with the general tectonic frame of the northeastern part of Africa, which is subjected to tensional stresses due to the rifting of the northern Red Sea and its northern branches (the Gulf Suez and Aqaba). By analyzing fault mechanism solutions in the Delta region and comparing them with the earthquake under study, we've found that the fault structures in the Hinge Zone and Cairo-Suez share similarities. This similarity provides evidence that the geodynamic processes and geological structures are identical.

The spectral method provides valuable information on the source of the seismic event and related energy distribution in the frequency domain using the FFT, as shown in Sect. 5.2. The idealized displacement spectra for body waves can be characterized by a flat part at lower frequencies and a fall-off above a corner frequency. The average seismic moment and moment magnitude values for P and SH waves are 1.85E+14Nm and Mw3.5, respectively. Furthermore, the average source values of radius and stress drop were calculated to be 304 m and 29 bar, respectively. The value of stress drop along the fault is relatively high, agreeing with that of the CSSZ earthquake of 7 July 2005, ML = 4.2. Both events indicate a relatively high stress drop value compared with the Cairo earthquake in October 1992 ($\Delta\sigma$ = 20 bar, Hussein 1999) and that for 1999, 2006

($\Delta\sigma = 10$ bar Abou Elenean and Hussein 2008). Abou Elenean et al. (2010) argued these relatively higher values to the high strength of the rocks along this belt.

Over the past few decades, numerous seismotectonic studies have been conducted in Egypt (e.g., Hussein et al. 2013; Sawires et al. 2015). The seismotectonic models for Egypt indicate that, there are a number of seismotectonic zones surrounding the Nile Delta (e.g. CSSZ, the northern and southern Gulf of Suez, Dahshour zone, Continental margin zones). An extensional and or extensional strike slips stress regime dominate these zones. These findings are agreed with the kinematics of the Red Sea -Gulf of Suez rift and Gulf of Aqaba transform plate boundary. Hassan et al. (2021) highlighted several challenges in investigating the tectonic setting of the eastern Mediterranean Basin, particularly the Nile Delta. These include the thick sedimentary cover, uncertainties in crustal and mantle velocities due to limited seismic stations, sparse seismic activity, and the scarcity of formation outcrops and deep wells for characterizing subsurface lithologies.

However, characterizing seismogenic sources requires integrating various types of data, including geological, seismicity, GPS, and geophysical data. Therefore, future efforts to characterize the seismotectonic setting of the Nile Delta are recommended. Such endeavours should utilize available information from local and regional geology, satellite imagery, Digital Elevation Models (DEMs), present-day tectonics, geodetic maps, paleoseismological studies, geophysical methods, updated seismological records, and updated focal mechanism data. Finally, this earthquake is a significant alarm for the region, highlighting the potential for future seismic events. However, it is crucial to emphasize that the continuous expansion of the seismic network in Egypt necessitates further extension towards the Nile Delta region. This extension is necessary to effectively monitor microseismicity and better understand seismic activity in the area. By expanding the seismic network to the Nile Delta, we can enhance our ability to detect and analyze smaller seismic events, providing valuable insights into the seismic behavior of the region.

Acknowledgements The authors want to thank Dr. Angela Saraò, the Editor of Journal of Seismology and the anonymous reviewers for their valuable comments, suggestions, and the critical and fruitful discussions that greatly improved the manuscript. Also, we would like to express our sincere gratitude to the Egyptian National Seismic Network-ENSN (DOI: 10.7914/SN/EY) and the Strong Motion Network for providing the valuable earthquake data used in our work. The availability of this data has been essential in conducting our research and enhancing our understanding of seismic events in the region. We extend our appreciation to the dedicated teams involved in operating and maintaining these networks, whose efforts have contributed to the advancement of seismic monitoring and hazard assessment in Egypt.

Author contribution In the research article, the authors made the following contributions: 1. Conception and Design: Abu El Nader, Hassan, and Badreldin were involved in formulating the research idea, conceptualizing the study objectives, and designing the research methodology. 2. Data Collection: Badreldin, Othman, Abu El Nader, Hassan and Adly collected the necessary data for the study, which may include seismic data, geological information, or other relevant data sources. 3. Data Analysis: Abu El Nader, Badreldin, and Othsman performed data analysis using appropriate statistical or analytical methods. This may involve processing seismic data, calculating seismic parameters, conducting spectral analysis, or applying other relevant techniques. 4. Interpretation of Results: Abu El Nader, and Hassan interpreted the findings of the data analysis, drawing meaningful conclusions and insights related to the research objectives. 5. Manuscript Writing: Abu El Nader, Badreldin, Othman and Hassan contributed to the writing of the manuscript, including drafting the introduction, methods, results, and discussion sections. They ensured the clarity and coherence of the written content. 6. Revision and Editing: Abu El Nader, Badreldin, Othman, Adly and Hassan participated in the revision and editing process, incorporating feedback from co-authors and reviewers to improve the quality and clarity of the manuscript. 8. Supervision and Guidance: Abu El Nader and Hassan provided supervision and guidance throughout the research process, offering valuable input, feedback, and oversight.

Data availability The seismic data in this study was provided by the Egyptian National Seismic Network in 2021-ENSN (DOI: 10.7914/SN/EY).No funding was obtained for this study.

Declarations

Competing interests The authors declare no competing interests.

Appendix A

Table 4 The geographical coordinates, elevation, sensor and digitizer type, polarities for seismic stations used in the estimation of seismological parameters for the Hinge Zone earthquake. U = Up polarity, D = Down polarity, HRD = High Resolution Digitizer, SS1 = Ranger Seismometer and STS-2 = Streckeisen STS-2 Broadband Sensor

Station	Latitude (°N)	Longitude (°E)	Polarity	Elevation (m)	Sensor type	Digitizer type
10th of Ramadan seismic station (RAM)	30.2170	31.8700	D	200	Trillium-120Q	RAM Trident
New SQARA seismic station (NSQR)	29.8830	31.2010	U	90	SS1	HRD
Kotamaya seismic station (KOT)	29.9280	31.8290	U	490	STS-2	Trident
Natrun seismic station (NAT)	29.6330	30.6170	U	270	Trillium 120	Trident
Suez (SUZ)	29.8400	32.8320	U	268	SS1	HRD
Rayan seismic station (RYAN)	29.0820	30.2775	U	99	Trillium 120	Trident
NEW BeniSwef seismic station (NBNS)	28.6230	31.2940	U	300	Trillium-40	Trident
Tur1 seismic station (TR1)	28.0070	33.9520	D	274	Trillium-40	Centaur-3
Dahab (DHB)	28.7221	34.6188	D	19	SS1	HRD
Hurghada (HRG)	27.0520	33.6080	U	398	Trillium-240	Trident305
Eilat (EIL)	29.6600	34.9500	U	210	STS-2	Quanterra Q330
Santkatherine (KAT)	28.5230	33.9930	D	1729	Trillium-40	Trident
Tur2 seismic station (TR2)	33.7230	28.3850	D	239	Trillium Compact	Taurus_3561
El Dabaa Seismic Station (NDB3)	31.0378	28.5482	U	100	Trillium-40	Trident
Helwan strong motion station (HKHLW)	29.8500	31.3400	U	140	Titan	Titan
Bnha strong motion (TBNH)	30.4600	31.1800	U	50	Titan	Titan
Dabaa strong motion station (TDAB)	31.0000	28.2800	D	100	Titan	Titan
Zoneima seismograph (ZNM)	29.3761	32.8752	U	201	Trillium Compact	taurus
Mayadin seismograph station MYD	29.7958	30.8009	U	279	L4C	HRD

References

Abd El-Aal AEAK, Tarabees E, Badreldin H (2017) Source characterization and ground motion modeling computed from the 3 September 2015 earthquake, western desert. Egypt Int J Geomate 12(30):166–174

Abd El-Aal, A. E. A. K., Hagag, W., Sakr, K., Saleh, M., Abd El-Aal, A. E. A. K., Hagag, W., ... and Saleh, M. (2019). Seismicity, seismotectonics and neotectonics in Egypt. In The Geology of Egypt, 375–413. Cham: Springer International Publishing.

Abd-Allah AM, Aal MHA, Ghandour A (2012) Structural characteristics and tectonic evolution of the northwestern margin of the Nile Delta. Egypt J Afr Earth Sci 68:82–95

Abdel-Fattah AK (2009) Attenuation of body waves in the crust beneath the vicinity of Cairo Metropolitan area (Egypt) using coda normalization method. Geophys J Int 176(1):126–134

Abdullah H, El-Hady SM, Soliman MS, Ezzelarab M (2022) Development a local magnitude scale for South Egypt. J Afr Earth Sci 188:104478

Abercrombie R, Leary P (1993) Source parameters of small earthquakes recorded at 2.5 km depth, Cajon Pass, southern California: implications for earthquake scaling. Geophys Res Lett 20(14):1511–1514

Abou Elenean KM, Hussein HM (2008) The October 11, 1999 and November 08, 2006 Beni Suef Earthquakes, Egypt. Pure Appl Geophys 165:1391–1410

Abou Elenean KM, Mohamed AM, Hussein HM (2010) Source parameters and ground motion of the Suez-Cairo shear zone earthquakes, Eastern Desert. Egypt Nat Hazards 52(2):431–451

Abou Elenean K (1997) Seismotectonics of Egypt in relation to the Mediterranean and RedSeas tectonics. Ain Shams University, Egypt (**Ph. D. thesis**)

Abu El Nader IF (2010) Seismotectonic of Egypt in view of an updated earthquake catalogue. Mansoura University, Egypt (**Ph.D thesis, Faculty of Science**)

Abu El Nader IF, El Gabry MN, Hussein HM, Hassan HM, Elshrkawy A (2013) Source characteristics of the Egyptian Continental margin earthquake, 19 October 2012. Seismol Res Lett 84(6):1062–1065

Ali SM, Badreldin H (2019) Present-day stress field in Egypt based on a comprehensive and updated earthquake

focal mechanisms catalog. Pure Appl Geophys 176(11):4729–4760
Ali Sherif M (2011) Source characterizations of inland earthquakes in Egypt. Ain-Shams University, Cairo, Egypt (**Ph.D thesis**)
Ambraseys NN, Melville CP, Adams RD (1994) The Seismicity of Egypt, Arabia and the Red Sea: A Historical Review. Cambridge University Press, Cambridge
Anderson DL, Ben-Menahem A, Archambeau CB (1965) Attenuation of seismic energy in the upper mantle. J Geophys Res 70(6):1441–1448
Archuleta RJ, Cranswick E, Mueller C, Spudich P (1982) Source parameters of the 1980 Mammoth Lakes, California, earthquake sequence. J Geophys Res: Solid Earth 87(B6):4595–4607
Badawy A (1999) Historical seismicity of Egypt. Acta Geod Geophys Hung 34:119–135
Badreldin H, Toni M, El-Faragawy K (2019) Moment tensor inversion of small-to-moderate size local earthquakes in Egypt. J Afr Earth Sc 151:153–172
Barakat MK (2010) Modern geophysical techniques for constructing a 3D geological Model on the Nile Delta, Egypt, Dissertation. Technical University of Berlin. https://doi.org/10.14279/depositonce-2627
Barton N (2007) Near-surface gradients of rock quality, deformation modulus, Vp and Qp to 1km depth, vol 25. First Break, EAGE, pp 53–60
Baumbach M, Bormann P (2009) Determination of source parameters from seismic spectra. In New Manual of Seismological Observatory Practice (NMSOP). Deutsches GeoForschungsZentrum GFZ, pp 1–6
Boore DM, Boatwright J (1984) Average body-wave radiation coefficients. Bull Seismol Soc Am 74(5):1615–1621
Brune JN (1970) Tectonic stress and the spectra of seismic shear waves from earthquakes. J Geophys Res 75(26):4997–5009
Brune JN (1971) Correction: Tectonic stress and the spectra of seismic shear waves. J Geophys Res 76(20):5002
CAPMAS (2022) Central Agency for Public Mobilization and Statistics (Egypt). Retrieved from http://capmas.gov.eg/Pages/Publications.aspx?page_id=5104andYear=23332
Eaton JP (1970) HYPOLAYR, A computer program for determining hypocenters of local earthquakes in an earth consisting of uniform flat layers over a half space (No. 69-85). US Geological Survey
EGSMA S (1981) Geological map of Egypt, scale 1: 2,000,000. The Egyptian Geological Survey and Mineral Authority
El-Hadidy S, Mohamed Adel ME, Deif A, Abu El-Ata SA, Moustafa Sayed SR (2006) Estimation of frequency-dependent coda wave attenuation structure at the vicinity of Cairo Metropolitan area. Acta Geod Geophys Hung 41(2):227–235
El-Hadidy S (1995) Crustal structure and its related causative tectonics in Northern Egypt using geophysical data. Ain Shams University, Cairo, Egypt (**Ph.D. Thesis**)
El-Sayed A, Vaccari F, Panza GF (2001) Deterministic seismic hazard inEgypt. Geophys J Int 144(3):555–567. https://doi.org/10.1046/j.1365-1174246x.2001.01372.x
El-Sayed A, Vaccari F, Panza GF (2004) The Nile Valley of Egypt: a major active graben that magnifies seismic waves. Seismic Ground Motion in Large Urban Areas. pp 983–1002
García-García JM, Vidal F, Romacho MD, Martín-Marfil JM, Posadas A, Luzón F (1996) Seismic source parameters for microearthquakes of the Granada basin (southern Spain). Tectonophysics 261(1–3):51–66
Goldstein PAUL, & Snoke A (2005) SAC availability for the IRIS community. Incorporated Research Institutions for Seismology Newsletter, 7(UCRL-JRNL-211140)
Hammam A, Gaber A, Abdelwahed M, Hammed M (2020) Geological mapping of the Central Cairo-Suez District of Egypt, using space-borne optical and radar dataset. Egypt J Remote Sens Space Sci 23:275–285
Hanks TC, Wyss M (1972) The use of body-wave spectra in the determination of seismic-source parameters. Bull Seismol Soc Am 62(2):561–589
Harms J, Wray J (1990) Nile Delta. In: Said R (ed) The geology of Egypt. Balkema, Rotterdam, pp 329–343
Hassan S, Sultan M, Sobh M, Elhebiry MS, Zahran K, Abdeldayem A, Kamh S (2021) Crustal Structure of the Nile Delta: Interpretation of seismic-constrained Satellite-based Gravity data. Remote Sens 13(10):1934
Havskov J, Ottemoller L (2010) Routine data processing in earthquake seismology: with sample data, exercises and software. Springer Science and Business Media
Herrmann RB, Kijko A (1983) Short-period Lg magnitudes: instrument, attenuation, and source effects. Bull Seismol Soc Am 73(6A):1835–1850
Hofstetter A (2014) On the reliability of focal plane solutions using first motion readings. J Seismolog 18(1):181–197
Hussein HM (1999) Source process of the October 12, 1992 Cairo Earthquake. Ann Geofis 42:665–74
Hussein IM, Abd-Allah AMA (2001) Tectonic evolution of the northeastern part of the African continental margin. Egypt J Afr Earth Sci 33(1):49–68
Hussein HM, Abou Elenean KM, Marzouk IA, Korrat IM, El-Nader IA, Ghazala H, ElGabry MN (2013) Present-day tectonic stress regime in Egypt and surrounding area based on inversion of earthquake focal mechanisms. J Afr Earth Sc 81:1–15
Jagger L, Bevan TG, and McClay KR (2018). Tectono-stratigraphic evolution of the SE Mediterranean passive margin, offshore Egypt and Libya. In: McClay KR, Hammerstein JA (eds) Passive Margins: Tectonics, Sedimentation and Magmatism. Geological Society, London, Special Publications, London. https://doi.org/10.1144/SP476.10
Kanamori H (1977) The energy release in great earthquakes. J Geophys Res 82(20):2981–2987
Kennett BLN, Engdahl ER (1991) Traveltimes for global earthquake location and phase identification. Geophysical Journal International 105(2):429–465
Khalil SM, McClay K (2002) Extensional fault-related folding, northwestern Red Sea. Egypt J StructGeol 24(4):743–762
Kiszely M (2000) Attenuation of coda waves in Hungary. Acta Geod Geophys Hung 35:465–473
Klein, F. W. (2002). User's guide to HYPOINVERSE-2000, a Fortran program to solve for earthquake locations and magnitudes (No. 2002–171). US Geological Survey
Klinger Y, Rivera L, Haessler H, Maurin J-C (1999) Active faulting in the Gulf of Aqaba: new knowledge from the

Mw 7.3 earthquake of 22 November 1995. Bull Seismol Soc Am 89:1025–1036
Korrat IM, El Agami NL, Hussein HM, El-Gabry MN (2005) Seismotectonics of the passive continental margin of Egypt. J Afr Earth Sc 41(1–2):145–150
Korrat IM, Lethy A, ElGabry MN, Hussein HM, Othman AS (2022) Discrimination between small earthquakes and quarry blasts in Egypt using spectral source characteristics. Pure Appl Geophys 179(2):599–618
Korrat IM, Elgabry MN, Lethy A, Hussein HM, Yavuz E, Othman AS (2023) Discrimination of quarry blasts from earthquakes in Northern and Central Egypt using linear and quadratic discriminant functions. J Seismolog 27(4):609–626
Kumar A, Kumar A, Mittal H, Kumar A, Bhardwaj R (2012) Software to Estimate Earthquake Spectral and Source Parameters. Int J Geosci 3:1142–1149
Lahr, J.C, (1980). HYPOELLIPSE: a computer program for determining local earthquake hypocentral parameters, magnitude and first motion pattern, U.S. Geological Survey Open-File Report 80–59, 59
Lee, W. H. K., and Lahr, J. C. (1972). HYPO71: A computer program for determining hypocenter, magnitude, and first motion pattern of local earthquakes, U.S. Geological Survey Open-File Report
Loncke L, Gaullier V, Mascle J, Vendeville B, Camera L (2006) The Nile deep-sea fan: an example of interacting sedimentation, salt tectonics, and inherited subsalt paleotopographic features. Mar Pet Geol 23:297–315. https://doi.org/10.1016/j.marpetgeo.2006.01.001
Mascle J, Benkhelil J, Bellaiche G, Zitter T, Woodside J, Loncke L (2000) Marine geologic evidence for a Levantine-Sinai plate, a new piece of the Mediterranean puzzle. Geology 28:779–782
Moustafa A, Abd-Allah A (1992) Transfer zones with en echelon faulting at the northern end of the Suez rift. Tectonics 11:499–509
Moustafa SSR, Abdalzaher MS, Abdelhafiez HE (2022) Seismo-Lineaments in Egypt: Analysis and Implications for Active Tectonic Structures and Earthquake Magnitudes. Remote Sens. 14:6151. https://doi.org/10.3390/rs14236151
NRIAG (2010) Historical seismicity of Egypt. A study for previous catalogues producing revised weighted catalogue the second arab conference for astronomy and geophysics. Egypt. https://www.nriag.sci.eg/
Rashwan M, Sawires R, Radwan AM, Sparacino F, Peláez JA, Palano M (2021) Crustal Strain and Stress Fields in Egypt from Geodetic and Seismological Data. Remote Sens 13(7):1398
Ross, D. A., and Uchupi, E. (1985). Continental Margin off Egypt: Structural Framework and Stratigraphic Evolution. In The Ocean Basins and Margins,(8) 369–387. Springer, Boston, MA. (from 869–871)
Ross DA, Uchupi E (1977) Structure and sedimentary history of southeastern Mediterranean Sea-Nile Cone area. AAPG Bull 61(6):872–902
Rybakov M, Voznesensky V, Ben-Avraham Z, Lazar M (2008) The Niklas anomaly southwest of Cyprus: New insights from combined gravity and magnetic data. Isr J Earth Sci 57:125–138
Said R (1990) The geology of Egypt: Rotterdam. Brookfield, Netherlands
Said, R (2012) The geological evolution of the River Nile. Springer Science & Business Media
Saleh M, Becker M (2015) New constraints on the Nubia–Sinai–Dead Sea fault crustal motion. Tectonophysics 651:79–98
Saleh M, Becker M (2019) New estimation of Nile Delta subsidence rates from InSAR and GPS analysis. Environmental Earth Sciences 78:1–11
Saleh, S. (2012). 3D crustal structure and its tectonic implication for Nile Delta and Greater Cairo regions, Egypt, from geophysical data. Acta Geodaetica et Geophysica Hungarica, 47(4). https://doi.org/10.1556/AGeod.47.2012.4.3
Sarhan MA, Collier LL, Basal A, Abdel Aal MH (2014) Late Miocene normal faulting beneath the northern Nile Delta: NNW propagation of the Gulf of Suez Rift. Arab J Geosci 7(11):4563–4571. https://doi.org/10.1007/s12517-013-1089-9
Sawires, R., Peláez, J. A., Fat-Helbary, R. E., Ibrahim, H. A., and García-Hernández, M. T. (2015). An updated seismic source model for Egypt. Earthquake engineering—from engineering seismology to optimal seismic design of engineering structures. InTech, Croatia, 1–51
Segev A, Sass E, Schattner U (2018) Age and structure of the Levant basin, Eastern Mediterranean. Earth Sci Rev 182:233–250
Sestini G (1989) Nile Delta: a review of depositional environments and geological history. Geol Soc Spec Publ 41(1):99–127
Shalaby A, Sarhan MA (2021) Origin of two different deformation styles via active folding mechanisms of inverted Abu El Gharadiq Basin, Western Desert. Egypt Journal of African Earth Sciences 183:104331. https://doi.org/10.1016/j.jafrearsci.2021.104331
Shalaby A, Sarhan MA (2023) Pre and post Messinian deformational styles along the northern Nile Delta Basin in the framework of the Eastern Mediterranean tectonic evolution. Marine Geophysical Research 44:22. https://doi.org/10.1007/s11001-023-09530-3
Singh SK, Apsel RJ, Fried J, Brune JN (1982) Spectral attenuation of SH waves along the Imperial fault. Bull Seismol Soc Am 72(6A):2003–2016
Skiple C, Anderson E, Fürstenau J (2012) Seismic interpretation and attribute analysis of the Herodotus and the Levantine Basin, ofshore Cyprus and Lebanon. Pet Geosci 18(4):433–442. https://doi.org/10.1144/petgeo2011-072
Snoke JA, Lee WHK, Kanamori H, Jennings PC, Kisslinger C (2003) FOCMEC: Focal mechanism determinations. International Handbook of Earthquake and Engineering Seismology 85:1629–1630
Stanley DJ (1988) Subsidence in the northeastern Nile delta: rapid rates, possible causes, and consequences. Science 240(4851):497–500
Suetsugu, D. (1998). Practice on source mechanism, International Institute of Seismology and Earthquake Engineering (IISEE) lecture note, Tsukuba, 104
Süle B, Wéber Z (2013) Earthquake source parameters and scaling relationships in Hungary (central Pannonian basin). J Seismolog 17(2):507–521
Tusa G, Gresta S (2008) Frequency-dependent attenuation of P waves and estimation of earthquake source

parameters in southeastern Sicily, Italy. Bull Seismol Soc Am 98(6):2772–2794

Watanabe K, Sato H, Kinoshita S, Ohtake M (1996) Source characteristics of small to moderate earthquakes in the Kanto region, Japan: application of a new definition of the S-wave time window length. Bull Seismol Soc Am 86(5):1284–1291

Zaghloul, Z.M., El-Gamai, M.M., Shaaban, F.F. and Yousef, A.F. (2001) Plates Interactions and Petroleum Potentials in the Nile Delta. Proceedings of the 1st Conference on the Deltas, Modern and Ancient, Cairo, 13–20 March 1999, 41–53